IX International Conference on Computational Methods in Marine Engineering
MARINE 2021
I.M. Viola and F. Brennan (Eds)

NUMERICAL INVESTIGATION OF PROPELLER INDUCED HULL PRESSURE PULSES USING RANS AND IDDES

MUYE GE*, URBAN SVENNBERG† AND RICKARD E. BENSOW*

*Chalmers University of Technology
Department of Mechanics and Maritime Sciences
Chalmers University of Technology, Gothenborg, Sweden
e-mail: muye.ge@chalmers.se; rickard.bensow@chalmers.se

† Kongsberg Hydrodynamic Research Centre
Varnumsleden 7, S-68193 Kristinehamn, Sweden
e-mail: urban.svennberg@km.kongsberg.com

Key words: Cavitation, Pressure Pulses, Tip Vortex Cavitation, IDDES, Marine Propeller

Abstract. This paper investigates the numerical predictions of pressure pulses induced by a cavitating marine propeller operating in behind-hull condition in model scale. Simulations are performed using the commercial package Star-CCM+ using RANS and IDDES approaches. The predicted sheet cavitation agreed well compared to experimental recordings and the 1st- and 2nd-order blade passing frequency (BPF) pressure pulses also agreed well compared to measurements via pressure transducers mounted on the model scale ship hull. Tip vortex cavitation (TVC) bursting was observed in the experiments and predicted as well in the numerical simulations. A traveling re-entrant jet from blade leading edge to blade tip was predicted underneath the sheet cavity structure, and triggered the partly collapse of sheet cavitation and strong TVC dynamics. The hull pressure fluctuations are found to be correlated with the rate of cavitation volume growth/shrinkage and the TVC dynamics are found generating high levels of higher-order BPF pressure pulses, according to the deduced TVC volume time series. Significant cavitation variations were recorded between blade passings and propeller revolutions in the experiments, while in the numerical predictions no noticeable cavitation difference was predicted, and the predicted 3rd- to 5th-order BPF pressure pulse tonal values are generally higher than experimental measurements. The cavitation variations in the experiments are suspected to be related with sheet cavitation inception rather than blade loading difference induced by wake dynamics.

1 INTRODUCTION

Propeller thrust is related to the pressure differences created on the two sides of the propeller blades via its rotational motion. This results in a rotating spatial distribution of pressure that generates pressure variations on the ship hull body, which is one of the major sources of hull vibration and on-board noise, as well as pressure waves in the surrounding medium. The pressure

on the propeller blades can drop below water saturation pressure and tension force can break the water medium, known as cavitation, contributes significantly to these side effects.

The 1st- and 2nd-order BPF pressure pulses are related to propeller blade thickness and loading and the growth/shrinkage of blade sheet cavitation for cavitating conditions. For 3rd- and higher-order BPF fluctuations it is widely believed to be induced by tip vortex cavitation related phenomenon indicated by various experimental studies. The tip vortex cavitation bursting was found to contribute substantially regarding hull pressure pulses [1] and in the experimental study in [2] the tip vortex bursting was found to be significantly influenced by the wake and its peak that the propeller was operating in. The phenomenon is found to be influenced by the mechanism that is termed 'sheet cavity closure' in the studies by [3]. The TVC bursting could be highly influenced by the re-entrant flow induced by sheet cavity collapse, and the TVC destruction by sheet cavity collapse is very common on ship propellers [4]. In [5] various possible mechanisms were discussed regarding tip vortex cavitation induced pressure pulses.

Viscous CFD code has been used for predicting cavitation and induced hull pressure pulses with cavitation mass transfer models. A RANS approach has been found to give satisfying predictions of sheet cavitation and 1st- to 2nd-order BPF hull pressure pulses, and scale resolving simulation approaches have been used for the prediction of tip vortex cavitation dynamics and higher-order pressure pulses [6, 7, 8, 9]. For these numerical predictions where higher-order pressure pulses are predicted, the propeller is operating in a wake generated by the ship hull or by upstream meshes, and the tip vortex cavitation bursting is also reported. As a continuation of [10], in the present study, numerical simulations are conducted for a model scale marine propeller operating behind a container vessel using the RANS and IDDES approaches. The container vessel is a generic 3600 TEU standard container vessel with representative design, and was used in the VIRTUE (The Virtual Tank Utility in Europe) and SONIC (Suppression Of under-water Noise Induced by Cavitation) EU projects. Model scale experiments were performed inside the large-size cavitation tunnel HYKAT in HSVA (Hamburgische Schiffbau Versuchsanstalt), including pressure pulse measurements and cavitation pattern recordings. Numerical predictions are presented from simulations using the commercial package Star-CCM+ (v2020.1).

2 Numerical methods

The governing flow equations are solved using the commercial package Star-CCM+ in a segregated manner. The RANS $k-\omega$ SST turbulence model, and the IDDES hybrid model based on the $k-\omega$ SST turbulence model are used. The Schnerr-Sauer mass transfer model [11] is used for cavitation prediction with the single fluid homogeneous mixture approach, and the two incompressible phases, water and vapor, are represented by the VoF (Volume of Fluid) with parameters α_l and α_v, respectively. For each simulation, MRF (Multiple Reference Frame) was used first, for a steady-state converged solution with $k-\omega$ SST turbulence, then follows with first-order implicit time advancing scheme and larger time steps with RBM (Rigid Body Motion). Implicit second-order Euler upwind time scheme is switched on with smaller time steps for another 6 propeller revolutions, and switched to IDDES for another 6 propeller revolutions. With the developed flow, the cavitation model is activated with gradually increased vaporization factor C_v and after that, the cavitating condition predictions are collected. The convection of velocity in the momentum equation is discretizatized using second-order schemes, which are

second order upwind for RANS and hybrid bounded central differencing for IDDES. Second order upwind scheme is used for turbulence terms. For the convection of vapor fraction α_v, the first order upwind scheme is used according to [11].

3 Simulation Design

The main geometrical information of the container vessel is summarized in table 1. The model scale container vessel (scale ratio $\lambda = 29.1$) was tested inside the largest cavitation tunnel HYKAT sized 2.8 m $\times$ 1.6 m $\times$ 11 m. The free-surface was substituted by wooden plates and the model scale vessel was installed with the even-keel design draft of $11.3/\lambda$ m with 50 mm margin to compensate for the tunnel ceiling boundary layer. The propeller rotation speed was fixed to $n = 28$ rps, with resulting blade Reynolds number of 3.1×10^6 based on blade chord length at 0.75 radius. The inlet velocity was adjusted to match the desired non-dimensional thrust coefficient $K_T = 0.2234$. The pressure was adjusted to the cavitation number $\sigma = 0.2354$, matched at 0.8 blade radius with 12 o'clock position. The thrust coefficient and cavitation number are defined as

$$K_T = \frac{T}{\rho n^2 D^4}; \quad \sigma = \frac{p - p_v}{0.5\rho(\pi n D)^2}, \tag{1}$$

in which T represents propeller thrust, ρ is water density and D is the model scale propeller diameter.

Totally 13 pressure transducers were mounted on the ship hull above the propeller, with arrangements shown in figure 1. The transducers were of the strain gauge type (Kulite XTM 190) with suitable frequency range up to 50 kHz, and a low pass filter was used for the amplifier and the resulting frequency range was limited to maximum of 1 kHz and the first five orders of BPF pressure pulses were reported.

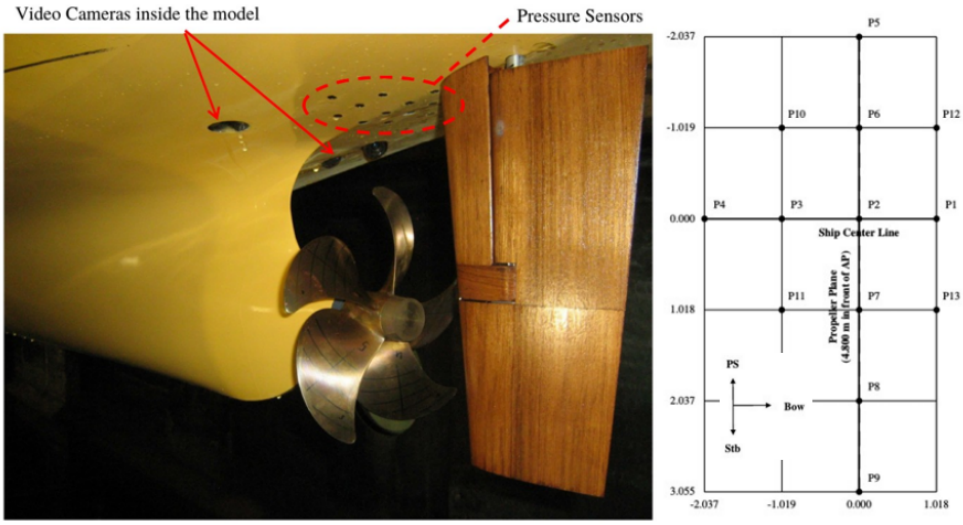

Figure 1: Pressure transducer arrangements in the experiments.

The simulation domain is chosen to be the same as the experimental test section, shown in the first frame in figure 2. The test section tunnel walls, ship body and propeller surfaces are set to no-slip walls and the inlet velocity, which is assumed to be uniform inlet, was adjusted to 7.1 m/s to match the desired K_T. The simulation domain is split into different regions, and the inner rotation region encloses the rotating propeller with a cylindrical sliding interface, to account for the rigid body motion of the propeller. The outer region encloses the rest of the space inside the tunnel section. There are 40 layers of prism cells with growth ratio of 1.15 on the propeller blades with target $y+ = 1$. The blades are meshed according to previous knowledge of sheet cavitation location with refinements of the tip vortex region, extending downstream about one chord length from the blade tip. On the ship hull, 38 layers of prism cells are applied with uniform growth ratio of 1.2 with target $y+ = 1$, and the aft-body was refined for better prediction of the propeller inflow. The aft-body and propeller grids are shown in the second frame in figure 2. There are in total 66.9 million cells including 38.7 million cells in the propeller rotation region and 28.2 million cells in the outer region. The mesh was generated using the STAR-CCM+ built-in polyhedral mesher.

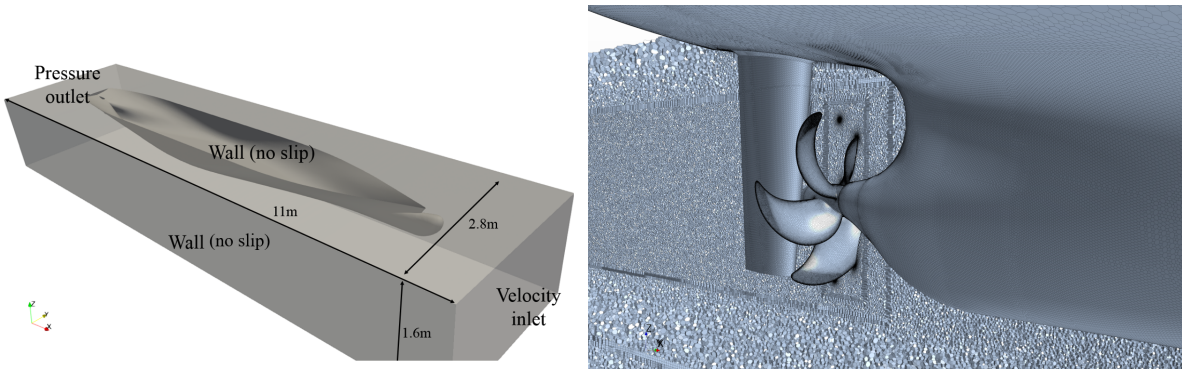

(a) Simulation domain and boundary conditions (b) Close up view of grids on the ship aft body

Figure 2: Simulation domain and computational grids.

4 Cavitation pattern prediction

The predicted cavitation patterns using IDDES and comparison with experimental observations are shown in figure 3. It can be noted that in the experiments, the camera shooting frequency were set to orders of propeller revolution, and variations of cavitation pattern between revolutions can be found for the same blade position in the recorded video. These variations can be found on all the blades while there is no phenomenal differences between the blades, thus the differences are believed not likely to be induced by manufacture deficiencies or assembling inaccuracy of pitch angles. Thus, representative frames of the experimental recording are selected and shown, with blade angle from 0 degrees at 12 o'clock position and increasing anti-clockwise viewing from the upstream side.

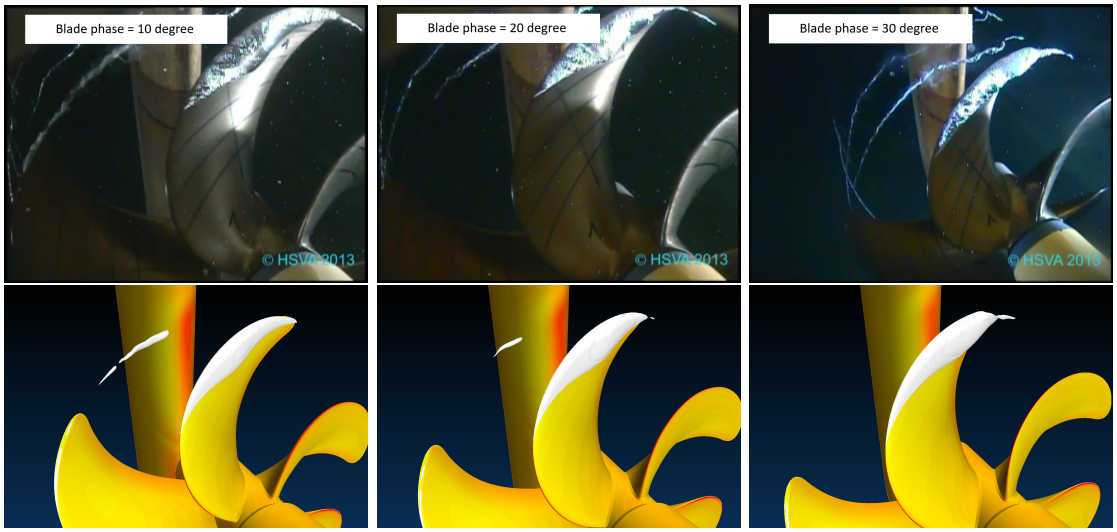

(a) 10 deg (b) 20 deg (c) 30 deg

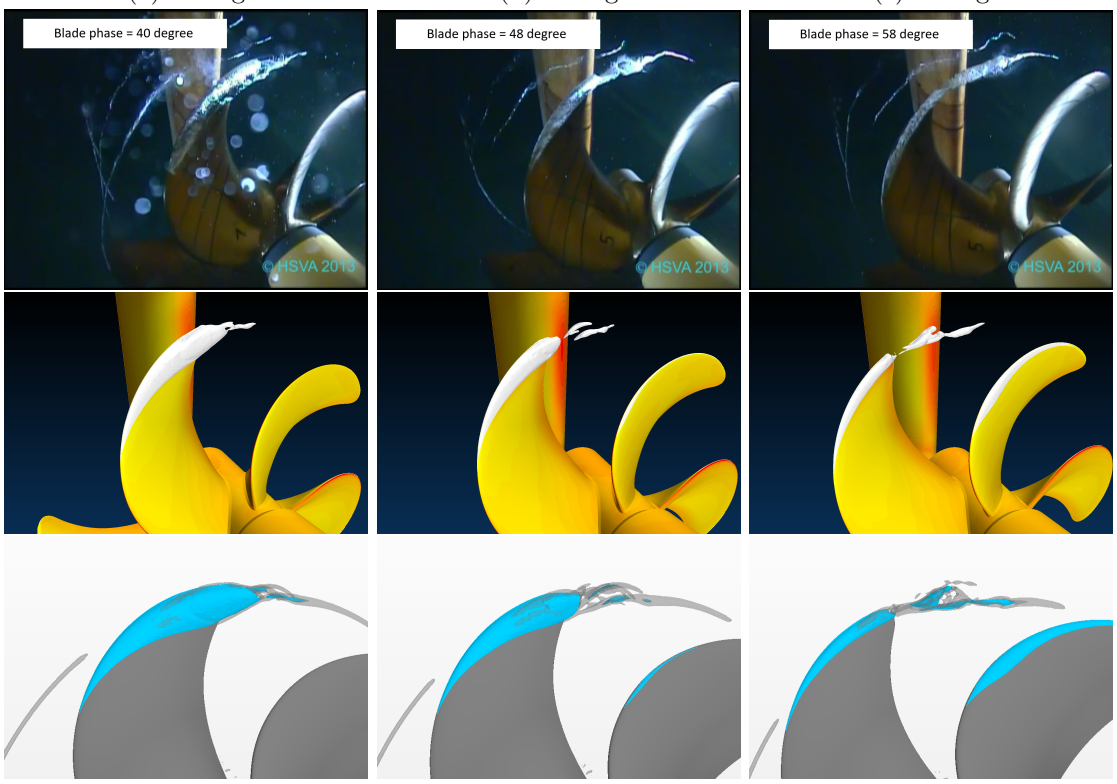

(d) 40 deg (e) 48 deg (f) 58 deg

Figure 3: Predicted cavitation patterns using Star-CCM+ and comparison with experimental recordings.The iso-surfaces of $Q = 5 \times 10^6$ are shown for the last three blade positions.

It can be found that sheet cavitation is the pronounced cavitation phenomena. In the experiments, the cavity interface is sharp and clear with a convex shaped vapor structure can be found moving from the blade leading edge to the blade trailing edge, shown at 10, 20, 30, 40 degrees. Around 40 degrees to 48 degrees, coincident with the time when the convex shaped part of vapor structure reaches the blade tip end, the tip vortex cavitation starts to develop significantly and become quite unstable, 'bursting', displaying a rather complex flow dynamics. After that, the tip vortex cavitation is back to a relatively stable state after blade phase of 58 degrees. The numerical predictions of sheet cavitation agree well compared to experimental recordings, especially the convex shaped closure line of the sheet cavitation is captured. The tip vortex cavitation is captured qualitatively well, with a shorter extent downstream compared to experimental observations. The complex multi-rolling TVC structures are predicted at around 48 degrees as well as the local thickening at around 58 degrees.

The re-entrant jet can be observed beneath the sheet cavitation, shown in figure 4 with the cavity structures rendered transparently and line contours of propeller upstream inflow U_x/U_{in}. The convex shaped sheet cavitation closure line can be found at relatively early stage of the formation of sheet cavitation around uppermost position at 0 degrees. The maximum extents of the sheet cavitation can be found at about the central line where the lowest value of U_x/U_{in} are located. The re-entrant jet underneath the sheet cavity can be first observed at blade position at about 10 degrees, and travels to the blade tip with the increase of blade degrees. At blade position of 40 degrees, the re-entrant jet reaches the blade tip and a large portion of sheet cavity close to the blade tip can be found detached from the blade surface. The aft-part of sheet cavitation thus collapse and tip vortex cavitation starts to form, shown in the last three frames in figure 4.

The re-entrant jet was studied in detail in [12], while the cavitation interface can be interpreted as a surface of constant pressure, with re-entrant jet perpendicular to the sheet cavitation closure line, and the twisted geometry of a hydro-foil may lead to the convergence of re-entrant jets and partly collapse of sheet cavitation. For the present case, the sheet cavitation is a rotating structure, while the re-entrant jet can still be related to the sheet cavity closure line as well as the propeller upstream inflow. The gradient of the propeller inflow can be interpreted as the density of the line contours, and the maximum curvature of sheet cavity closure line are located besides the central line with maximum $grad(U_x/U_{in})$ where high density of contour lines are located.

The cavitation pattern development can be correlated with the predicted pressure fluctuation signal, which is shown in the first frame in figure 5 for the pressure fluctuation recorded on transducer No. 7, for 5 blade passings. There are 4 dashed red vertical lines marking the major cavitation events, corresponding to blade phases of 40, 48, 58 and 82(10) degrees. For a monopole, the far-field pressure fluctuation is proportional to its volumetric variation, i.e. the second-order derivative of its volume with respect to time,

$$p' \approx \frac{\rho}{4\pi r}\frac{\partial^2 V_{b(t-r/c)}}{\partial t^2}, \tag{2}$$

in which r represents the distance between the monopole and the receiver point, t is time, c is the velocity of pressure wave and V_b represents the volume of the monopole. In order to investigate the relationship between induced pressure pulses and cavitation dynamics, the

predicted vapor volume was calculated during the simulation as $V_{total} = \sum \alpha_{v,i} V_{celli}$. It is also of interest to isolate the vapor volume of the tip vortex cavitation from the sheet cavitation, which can be achieved by selecting the cells with wall distance larger than 2 cm, which excludes the sheet cavitation and lead to the deduced vapor volume of tip vortex cavitation. The total vapor volume V_{total} and the deduced tip vortex cavitation vapor volume V_{TVC} are plotted in the second frame in figure 5 in black and blue lines respectively. Accordingly, the term d^2V/dt^2 can be calculated for the total vapor volume V_{total} and TVC vapor volume V_{TVC}, shown in the third and fourth frames in figure 5. The calculated d^2V_{total}/dt^2 highly agree with the recorded hull pressure fluctuation. The maximum total vapor volume is about 4 cm^3 while the tip vortex vapor volume is much smaller with maximum value smaller than 0.5 cm^3. However, even though the V_{TVC} is smaller, TVC induced pressure pulses are very pronounced and rich in higher-order BPF.

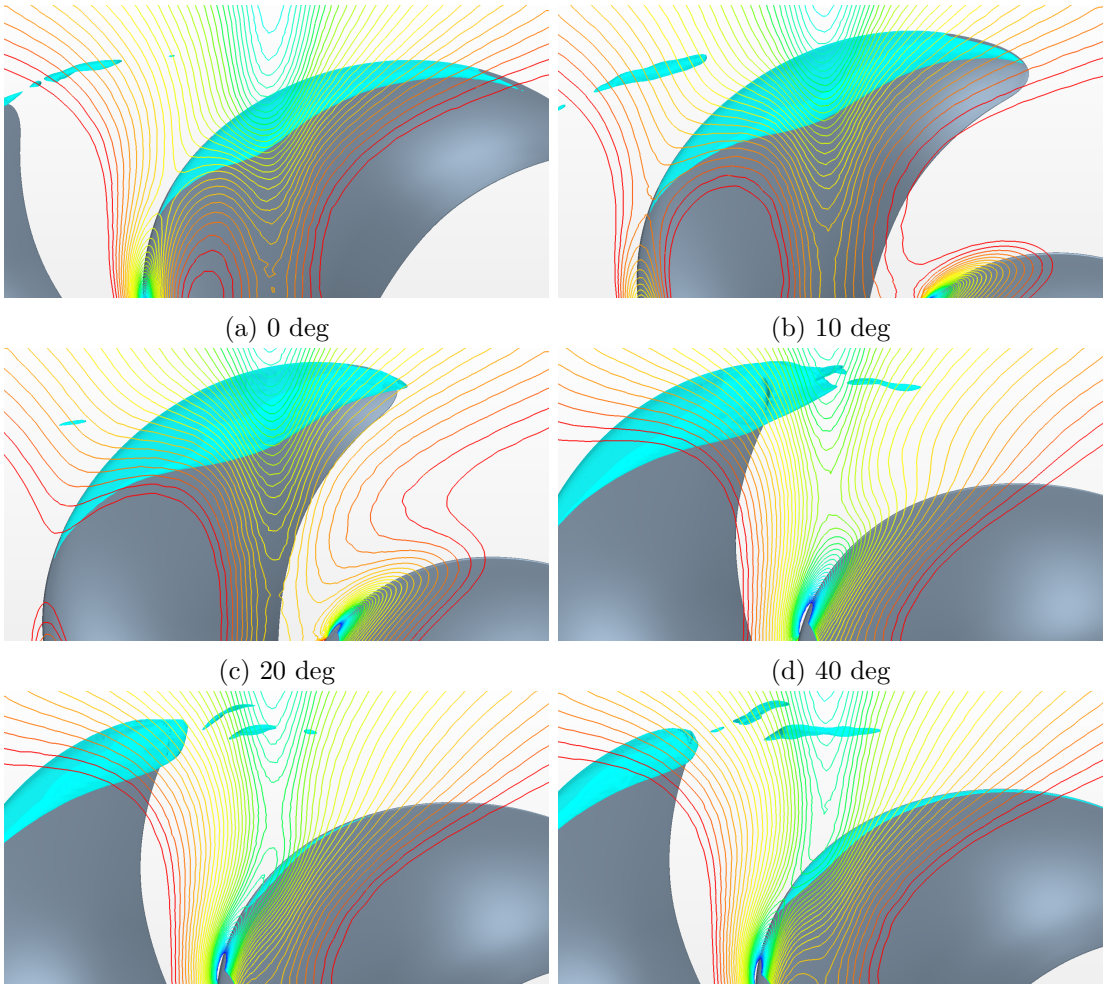

(a) 0 deg (b) 10 deg

(c) 20 deg (d) 40 deg

(e) 48 deg (f) 52 deg

Figure 4: Cavitation and re-entrant jet developments with propeller inflow (U_x/U_{in}) line contours.

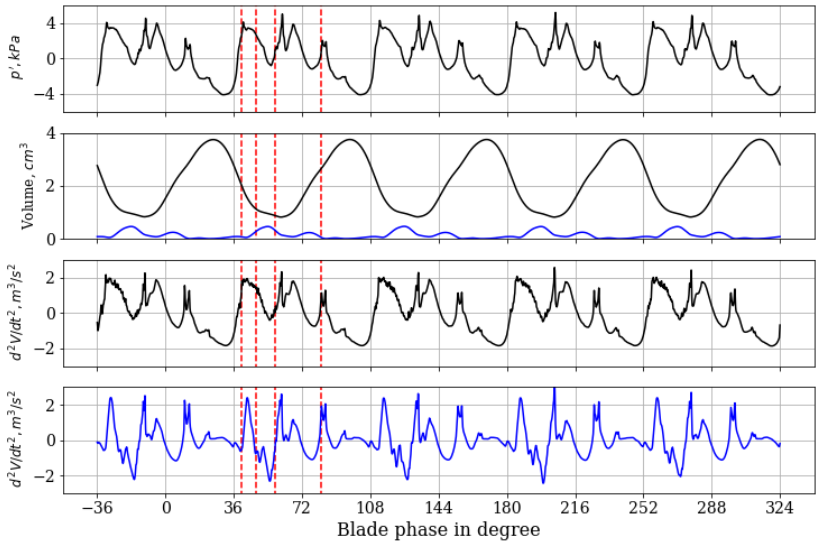

Figure 5: Recorded pressure fluctuation and vapor volumes. From top to bottom: frame 1, pressure fluctuation on transducer location No. 7; frame 2, integrated vapor volumes, total vapor volume V_{total} plotted in black line and deduced tip vortex cavitation volume V_{TVC} plotted in blue line; frame 3: rate of total vapor volume collapse/shrinkage (d^2V_{total}/dt^2); frame 4: rate of deduced tip vortex cavitation vapor volume collapse/shrinkage (d^2V_{TVC}/dt^2).

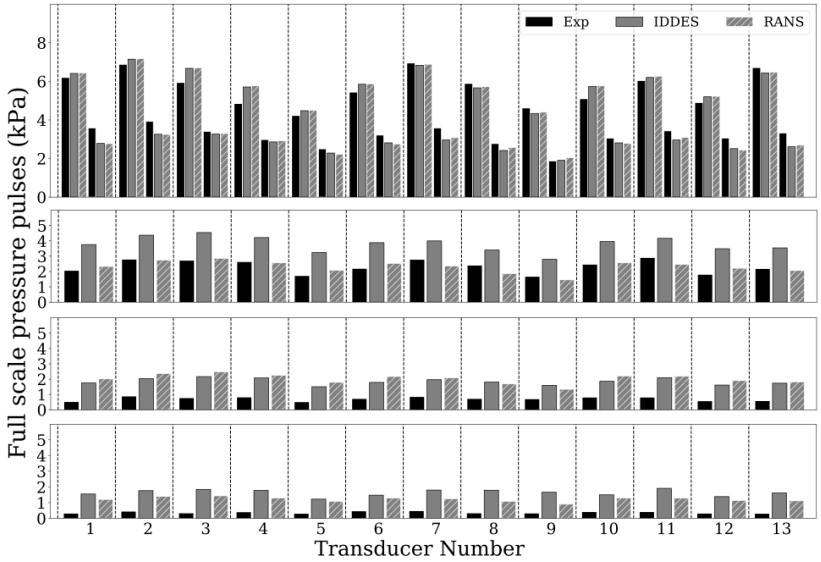

Figure 6: Predicted 1st- to 5th-order BPF pressure pulse levels using RANS and IDDES and comparison to experimental measurements. From top to bottom: pressure pulses in 1st- and 2nd-order BPF; 3rd-order BPF; 4th-order BPF; 5th-order BPF.

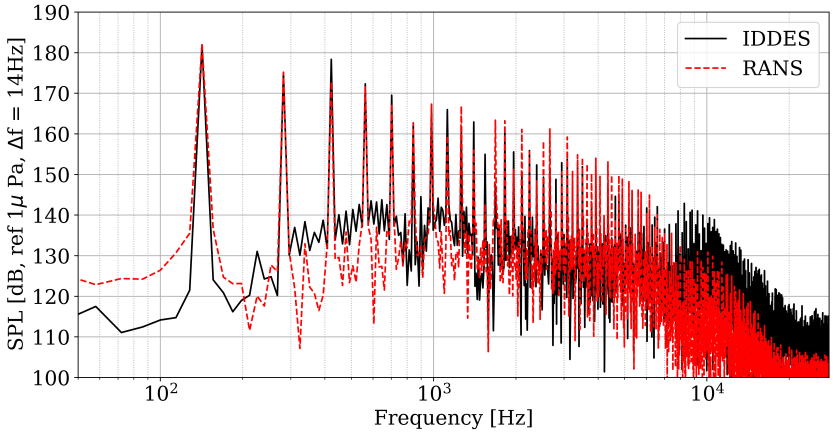

Figure 7: FFT spectrum of recorded model scale hull pressure on location transducer 7.

The pressure pulses predicted using IDDES and RANS are summarized in figure 6 from 1st-order BPF to 5th-order BPF with full scale values. The scaling from model scale values to full scale values is via a simple non-dimensional scaling, i.e. the non-dimensional coefficient K_p is calculated using model scale values and K_p is assumed to be constant between different scales as

$$K_p = \frac{p'_m}{\rho_m n_m^2 D_m^2}, \quad p'_s = K_p \rho_s n_s^2 D_s^2,$$

in which the subscript m and s represent model scale and full scale quantities, respectively. The FFT spectrum of IDDES and RANS predicted pressure fluctuation signals at transducer location No. 7 are shown in figure 7 based on predictions of 10 blade passings, with RANS prediction plotted in dashed red lines and IDDES prediction plotted in solid black line.

For 1st- and 2nd-order BPF pressure pulses, the numerical prediction agreed very well compared with experimental measurements for all the transducer locations. There are little difference between RANS and IDDES predictions. For higher orders the pressure pulses levels are generally over-predicted compared to experimental data, and IDDES predicted higher levels than RANS. This discrepancy can be related to the variation of cavitation phenomenon in the experiments, which will increase the broadband part of the spectrum and lead to lower tonal values at BPFs. The dynamic wake can be one of the reason that lead to propeller inflow dynamics and thus blade loading and cavitation variations. However, in the present study, the predicted propeller inflow dynamics are minor and not strong enough to induce noticeable blade loading and cavitation variations. By examining experimental recordings the variation can be related to sheet cavitation inception, shown in figure 8. The blades are in the same position for the three frames, while the difference of sheet cavitation inception can be found on the right hand side blade's leading edge. Apart from sheet cavitation inception shown in the first frame, there are instances that no sheet cavitation inception with traveling bubble cavitation showing up instead. This indicate the local pressure is below saturation pressure but sheet cavitation was not

developing. This phenomenon can be found in many model scale experiments with propellers mounted on inclined shaft, where the propeller inflow is largely uniform but large cavitation variations can be found between blade passings and revolutions. For the present case, cavitation inception differences can lead to different formation of sheet cavitation shape shown in figure 9 and furthermore, influence the formation of the underneath re-entrant jet, variations of sheet cavitation collapse as well as TVC formation and bursting, both in magnitudes and phases.

Figure 8: Instances of sheet cavitation inception (the right hand side blade).

Figure 9: Cavitation differences observed in the experiments.

4.1 Summary

Numerical simulations are performed for the prediction of a model scale cavitating propeller induced hull pressure pulses using commercial package Star-CCM+. The predicted sheet cavitation agreed well with experimental recordings using both RANS and IDDES. The 1st- and 2nd-order BPF pressure pulses also agreed well compared to experimental measurements for the 13 pressure transducer measurements. Tip vortex cavitation and bursting were observed during the experiments and predicted in the numerical simulations, which contribute to high levels of higher-order BPF hull pressure pulses. A re-entrant jet was found beneath the sheet cavitation and traveling from blade leading edge to blade tip, and triggered the partly violent collapse of sheet cavity and tip vortex cavitation generation and bursting. The formation of the re-entrant jet can be correlated to the convex shaped sheet cavity closure line and the propeller inflow. The predicted hull pressure pulse signal was found highly correlated with the rate of cavity growth/shrinkage, i.e. d^2V/dt^2. Similarly the tip vortex cavitation's contribution to pressure pulses was separated from sheet cavitation based on vapor volume separation. The major events found in the d^2V/dt^2 signal are correlated with the predicted cavitation phenomenon:

sheet cavitation start developing with the formation of re-entrant jet at about blade position of 10 degrees; the sheet cavitation grows and shrinks while re-entrant jet travels to the blade tip at about blade position of 40 degrees; after the re-entrant jet's arrival to the blade tip, part of sheet cavity collapse violently with generation of complex tip vortex cavitation, formed the first pressure pulse signal peak; the collapse of tip vortex cavitation formed the second pronounced signal peak at about blade position of 58 degrees and rebounds, and a second significant collapse can be found at blade position of 82(10) degrees. Comparing to experimental measurements, the 3rd- to 5th-order BPF pressure pulses are generally over-predicted, which is believed due to cavitation variations between blades and revolutions in the experiments that increase the spectrum broadband parts and reduce the tonal values at BPFs. In numerical predictions, no significant propeller inflow dynamics were predicted and the predicted cavitation patterns are highly repeatable between blades and revolutions. Thus it is suspected that the sheet cavitation inception differences observed in the experimental recordings lead to the cavitation variations and not captured in the numerical simulations.

5 Acknowledgement

We would like to thank HSVA for sharing geometry and experimental data. Financial support for this work has been provided by Kongsberg Maritime Sweden AB through the University Technology Centre in Computational Hydrodynamics hosted at the Department of Mechanics and Maritime Sciences at Chalmers University of Technology. The computations were performed on resources at Chalmers Centre for Computational Science and Engineering (C3SE) and National Supercomputer Centre (NSC) at Linköping University provided by the Swedish National Infrastructure for Computing (SNIC).

REFERENCES

[1] J. English, "Cavitation induced hull surface pressures–measurements in a water tunnel," 1980.

[2] A. Konno, K. Wakabayashi, H. Yamaguchi, M. Maeda, N. Ishii, S. Soejima, and K. Kimura, "On the mechanism of the bursting phenomena of propeller tip vortex cavitation," *Journal of marine science and technology*, vol. 6, no. 4, pp. 181–192, 2002.

[3] G. Bark and R. E. Bensow, "Hydrodynamic mechanisms controlling cavitation erosion," *International Shipbuilding Progress*, vol. 60, no. 1-4, pp. 345–374, 2013.

[4] G. Kuiper, "New developments around sheet and tip vortex cavitation on ships propellers," *http://resolver. caltech. edu/cav2001: lecture. 007*, 2001.

[5] E. van Wijngaarden, J. Bosschers, and G. Kuiper, "Aspects of the cavitating propeller tip vortex as a source of inboard noise and vibration," in *ASME 2005 Fluids Engineering Division Summer Meeting*. American Society of Mechanical Engineers, 2005, pp. 539–544.

[6] K. Fujiyama, "Numerical simulation of ship hull pressure fluctuation induced by cavitation on propeller with capturing the tip vortex," in *Fourth International Symposium on Marine Propulsors*, 2015.

[7] D. Li, J. Hallander, and R. Karlsson, "Progress in predicting pressure pulses and underwater radiated noise induced by propeller with pressure side cavitation," in *Numerical Towing Tank Symposium (NuTTS 2015), Cortona, Italy*, 2015.

[8] N. Sakamoto and H. Kamiirisa, "Prediction of near field propeller cavitation noise by viscous cfd with semi-empirical approach and its validation in model and full scale," *Ocean Engineering*, vol. 168, pp. 41–59, 2018.

[9] D.-Q. Li, J. Hallander, and T. Johansson, "Predicting underwater radiated noise of a full scale ship with model testing and numerical methods," *Ocean Engineering*, vol. 161, pp. 121–135, 2018.

[10] M. Ge, U. Svennberg, and R. E. Bensow, "Investigation on rans prediction of propeller induced pressure pulses and sheet-tip cavitation interactions in behind hull condition," *Ocean Engineering*, vol. 209, p. 107503, 2020.

[11] G. H. Schnerr and J. Sauer, "Physical and numerical modeling of unsteady cavitation dynamics," in *Fourth international conference on multiphase flow*, vol. 1. ICMF New Orleans, 2001.

[12] E.-J. Foeth, "The structure of three-dimensional sheet cavitation," *Delft University of Technology, Ship Hydromechanics Laboratory, Faculty 3mE, Department of Marine Technology, Doctors Thesis, Promotoren Prof. dr. ir. TJC van Terwisga en Prof. dr. ir. HWM Hoeijmakers, Printed by Ponsen en Looijen bv, Wageningen, The Netherlands*, 2008.